Sensors and Materials, Vol. 31, No. 4 (2019) 1167–1179
MYU Tokyo

S & M 1843

Facile Preparation of Hemin-functionalized Electrochemically Reduced Graphene Oxide Nanocomposite for H_2O_2 Biosensing

Zhi Chen, Dong Liu,* Chengxi Zhu, Libo Li, and Tianyan You**

School of Agriculture Equipment Engineering, Institute of Agricultural Engineering, Jiangsu University, 301 Xuefu Road, Zhenjiang, Jiangsu 212013, China

(Received August 30, 2018; accepted December 27, 2018)

Keywords: Hemin, electrochemically reduced graphene oxide, nonenzymatic biosensor, hydrogen peroxide

A Hemin-functionalized electrochemically reduced graphene oxide (H-ERGO) nanocomposite was prepared for the construction of a nonenzymatic H_2O_2 biosensor. H-ERGO was directly modified on the electrode surface without using a binder by electrochemical reduction. Detailed physical and electrical characterizations of H-ERGO were conducted by scanning electron microscopy, UV–vis absorption spectroscopy, and electrochemical impedance spectroscopy (EIS). Taking advantage of the superior catalytic properties of H-ERGO, we applied the proposed biosensor to H_2O_2 analysis. Under optimized conditions, the H-ERGO-based biosensor exhibited a wide linear range from 25 to 8850 and 8850 to 28850 μM, with a detection limit (S/N = 3) of 8.33 μM for H_2O_2 determination. Furthermore, it was also successfully applied to detect H_2O_2 in milk samples with recoveries ranging from 94.6 to 98.1%.

1. Introduction

Hydrogen peroxide (H_2O_2) is closely related to many vital physiological and biochemical changes in organisms. For instance, H_2O_2 in plants is essential for stress response and the regulation of programmed cell death, while mammalian cells generate H_2O_2 to mediate diverse physiological responses, including cell proliferation, differentiation, and migration.[1,2] In addition, H_2O_2 is of great importance in food processing, disinfection, and pharmaceutical production. Dairy industries widely use H_2O_2 as a preservative to prevent corruption and extend the shelf life of dairy products.[3] However, the residue of H_2O_2 can cause neurodegenerative disorders, cancer, diabetes, and other health problems.[4] Therefore, the accurate measurement of H_2O_2 level is very important. Traditional H_2O_2 determination methods include the colorimetric method,[5] fluorescence method,[6] flow injection method,[7] and electro-chemiluminescence.[8] However, the application of these methods is limited by a complicated, time-consuming, or expensive process. Moreover, these techniques require skilled operators and sophisticated instrumentation. It is generally accepted that the electrochemical method has many advantages, including fast response, cheap apparatus, simple operation, and high sensitivity and selectivity.[9] H_2O_2 can be reduced on ordinary electrodes; however, its

*Corresponding author: e-mail: dongliu@ujs.edu.cn
**Corresponding author: e-mail: youty@ujs.edu.cn
https://doi.org/10.18494/SAM.2019.2124

ISSN 0914-4935

sensitivity is low and it is easily interfered by other substances. Therefore, it is necessary to develop high-performance electrochemical sensors for H_2O_2 biosensing.

Hemin is a type of ferroporphyrin derivative and the active center of various heme proteins including hemoglobin peroxidase and myoglobin. Typically, a pair of reversible or quasi-reversible peaks from the redox of Hemin-Fe can be obtained in cyclic voltammograms.[10,11] Recent investigations have revealed that Hemin can exhibit peroxidase-like catalytic activity towards the H_2O_2 reduction reaction; thus, many efforts have been devoted to the fabrication of Hemin-based H_2O_2 biosensors. For instance, Lotzbeyer *et al*. modified the cystamine monolayer to covalently bind Hemin on gold electrodes, which exhibited high electrocatalytic activity for H_2O_2 reduction.[12] Valentini *et al*. used carbon nanofibers (CNFs) to immobilize Hemin by π–π interactions. The open structure of CNFs coupled with a high surface functional group density enhanced the catalytic activity of Hemin, and the fabricated biosensor achieved a low detection limit for H_2O_2.[13] However, a binder, such as nafion or chitosan, is required to anchor the Hemin stably on electrodes or nanomaterials, which may complicate the fabrication procedure and limit further improvement of the analytical performance of Hemin-based biosensors.

Graphene oxide (GO), consisting of a single layer, has a large surface area and attractive mechanical properties. Abundant oxygen-containing functional groups on the surface of GO favor its surface functionalization.[14] The reduction of GO is a significant method for the preparation of graphene, and investigations focused on reduced graphene oxide (rGO)-based sensors have received extensive attention. For example, Zhou *et al*. fabricated 1-aminoindole functionalized rGO on electrodes to measure phenolic substances.[15] Chen *et al*. used rGO to construct a molecular adsorption gas sensor for sensing NO_2 and NH_3.[16] Recently, the preparation of graphene by electrochemical reduction has been extensively studied. This method does not use a reducing agent, and the electrochemically reduced graphene oxide (ERGO) shows similar electrochemical performance to chemically reduced GO.[17] For the biosensor fabrication, ERGO can be directly modified on the electrode by electrochemically reducing GO without using any binder, which can simplify the fabrication procedure.

In this work, we have prepared a Hemin-functionalized electrochemically reduced graphene oxide (H-ERGO) nanocomposite to fabricate a nonenzymatic H_2O_2 biosensor. The immobilization of Hemin and the reduction of GO were accomplished simultaneously on the electrode surface. Under optimized conditions, the proposed biosensor exhibited a wide linear range with a detection limit (S/N = 3) of 8.33 μM for the detection of H_2O_2. It was also successfully used to detect H_2O_2 in milk samples.

2. Materials and Methods

2.1 Reagents and materials

GO was purchased from XFNANO Technology Co., Ltd. (Nanjing, China). Hemin (ferriprotoporphyrin IX chloride, 98 wt%) was purchased from Sigma. All other reagents used in this work were obtained from Sinopharm Chemical Reagent Co., Ltd. (Shanghai, China).

Milk bought from a local supermarket (Zhenjiang, China) was utilized for the real sample analysis. The ultrapure water supplied by a Milli-Q Plus system (Millipore) was used for all the solution preparations. All the experiments were conducted at room temperature.

2.2 Instrumentation

Scanning electron microscopy (SEM) images were taken on a S-3400N scanning electron microscope (Hitachi, Japan). UV–vis absorption and Raman spectra were obtained on a UV-2450 spectrophotometer (Shimadzu, Japan) and a DXR Raman microscope (ThermoFisher, USA), respectively. Electrochemical experiments were conducted on a CHI852D electrochemical workstation (Chenhua, China). The three-electrode system was used with a modified glassy carbon electrode (GCE) (diameter = 2 mm) as the working electrode, a platinum wire electrode as the auxiliary electrode, and a Ag/AgCl electrode (saturated KCl) as the reference electrode. Electrochemical impedance spectroscopy tests were performed on a Zennium electrochemical workstation (ZAHNER, Germany).

2.3 Preparation of Hemin-functionalized graphene oxide (H-GO)

For the preparation of H-GO, 30 mg of GO and 15 mg of Hemin were mixed in 15 mL of ultrapure water, followed by ultrasonication in an ultrasonic homogenizer for 30 min. Then, the solution was stirred for 24 h to obtain H-GO.

2.4 Preparation of H-ERGO

GCE was firstly polished with 0.05 μm alumina powder and sequentially sonicated in ethanol and ultrapure water, and then dried at room temperature. 2 μL of H-GO solution was cast on GCE and dried in air. Then, cyclic voltammetry (CV) was applied to reduce H-GO to H-ERGO/GCE in 0.1 M PBS (pH 7.0) in the potential range from 0.0 to −1.4 V for 50 cycles at a scan rate of 50 mV s^{-1}.[18]

3. Results and Discussion

3.1 Principles

To achieve the direct immobilization of Hemin without a binder during the biosensor fabrication, we developed a novel method of synthesizing H-ERGO on an electrode (Fig. 1). Briefly, Hemin was anchored on GO by π–π interactions, and the obtained H-GO composite was modified on the electrode. Then, the following electrochemical reduction can reduce GO to ERGO as well as anchor the nanocomposite on the electrode. Hemin in H-ERGO retained its catalytic activity toward H_2O_2 reduction; ERGO showed a high conductivity and a large effective specific surface area. The fabricated electrochemical biosensor based on H-ERGO showed superior analytical properties toward H_2O_2.

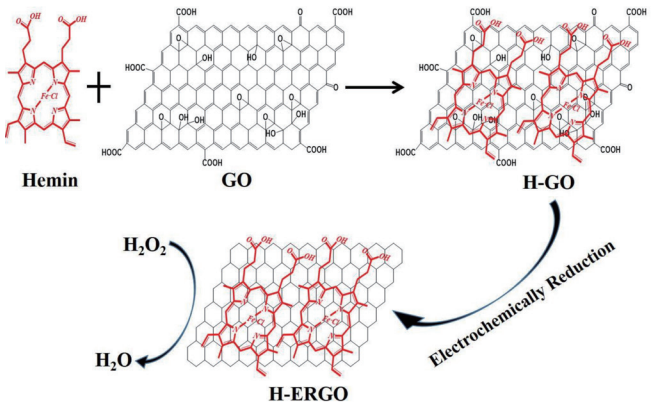

Fig. 1. (Color online) Schematic for the preparation of H-ERGO and its application to H_2O_2 detection.

3.2 Characterization of composite

The functionalization of Hemin on GO was characterized by UV–vis spectroscopy. Figure 2(a) shows the UV–vis spectra of GO, Hemin, and H-GO. The peak located at 225 nm for GO and H-GO was the typical characteristic absorption of GO derived from the π–π* transition of aromatic C=C bonds. Typically, the UV–vis spectra of Hemin display two characteristic absorption bands at 390 nm and a Q-band at 500–700 nm.[19] For H-GO, absorption peaks were observed at 240 and 410 nm, which were assigned to GO and Hemin, respectively. The redshifted peaks may originate from the π–π interaction between GO and Hemin.[20] Raman spectra were further obtained to characterize the crystal structures of carbon in H-GO and H-ERGO. As shown in Fig. 2(b), the results of Raman spectra show a D band at 1351 cm^{-1} and a G band at 1578 cm^{-1} for both H-GO and H-ERGO. Generally, the D band for carbon corresponds to the edge and disordered carbon atoms, reflecting the degree of disorder and defects, whereas the G band corresponds to the sp^2-bond carbon atoms, reflecting the degree of symmetry and crystallization.[21] Here, the calculated I_D/I_G values are 0.86 for H-GO and 1.11 for H-ERGO [Fig. 2(b)]. The relatively larger I_D/I_G value of H-ERGO demonstrated that most of the oxy-generated groups were removed and the proportion of sp^2 domains was reduced after the electrochemical reduction of GO, whereas the number of defects existing in H-ERGO is higher than that in GO.[22]

The morphologies of the electrodes were characterized by SEM. In Fig. 3(a), the SEM image shows the smooth surface of the GCE. For the GO-modified GCE (GO/GCE), the clearly observed wrinkle structure indicates the successful modification of GO [Fig. 3(b)].[23] The aggregation of Hemin with block structures could be observed on the Hemin-modified GCE (Hemin/GCE) [Fig. 3(c)]. According to the SEM image of the H-ERGO composite modified GCE (H-ERGO/GCE), relatively small blocks of Hemin aggregation are encapsulated by the graphene on the surface of the GCE; however, no distinguishable wrinkle for typical graphene structures is observed, which may be ascribed to the functionalization of Hemin on graphene [Fig. 3(d)].

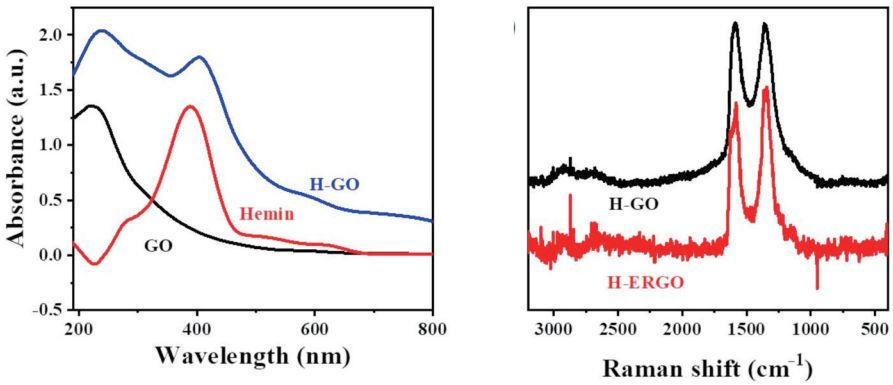

(a) (b)

Fig. 2. (Color online) (a) UV–vis absorption spectra of GO, Hemin, and H-GO. (b) Raman spectra of GO and H-ERGO.

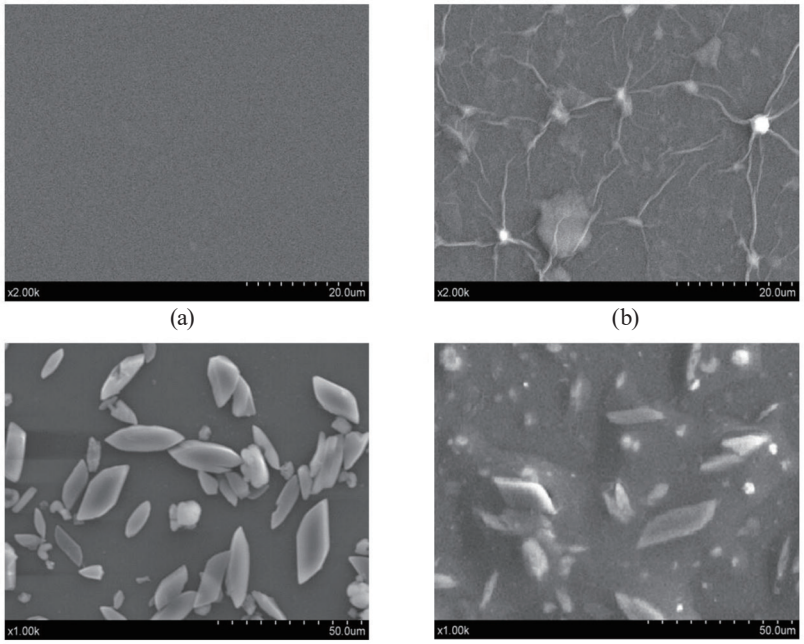

(a) (b)

(c) (d)

Fig. 3. SEM images of (a) GCE, (b) GO/GCE, (c) Hemin/GCE, and (d) H-ERGO/GCE.

3.3 Electrochemical behavior of H-ERGO

The electrochemical performance of H-ERGO was examined by CV and electrochemical impedance spectroscopy (EIS). Figure 4 shows the reduction of GO on H-GO/GCE and GO/GCE. After 50 cycles, compared with that of GO/GCE, the CV curve of H-GO/GCE shows a pair of distinct redox peaks at −0.35 V, which is ascribed to the redox reaction of Hemin-Fe.[23] The peak at −1.15 V disappears after 50 cycles of CV scanning for both H-GO/GCE and GO/GCE owing to the removal of oxy-generated groups from the GO surface.

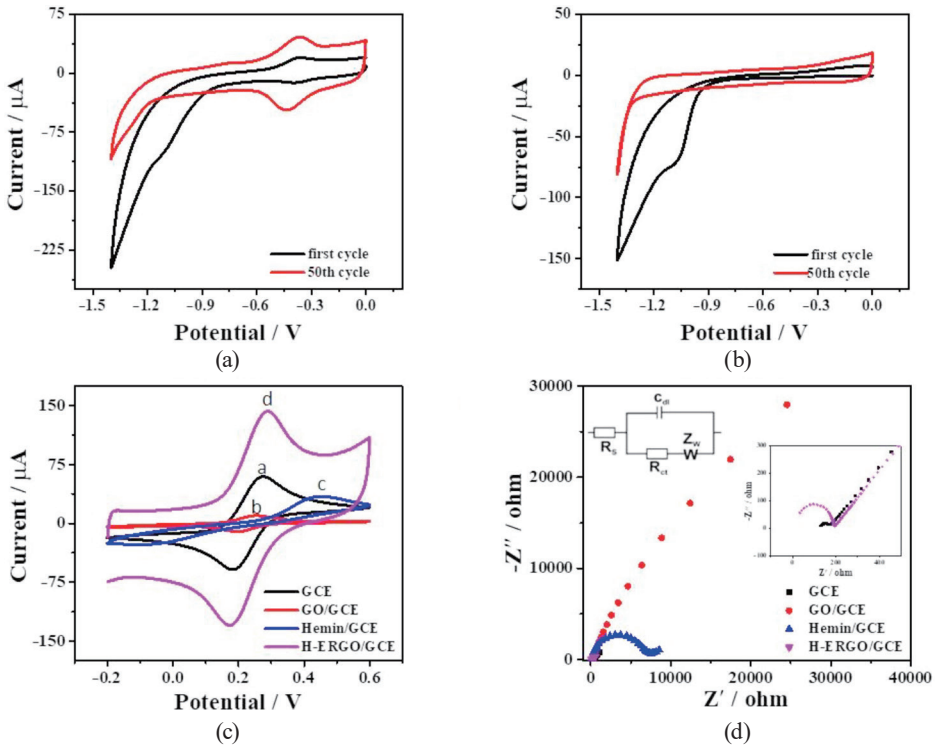

Fig. 4. (Color online) CV curves of (a) H-GO/GCE and (b) GO/GCE in 0.1 M PBS (pH 7.0) for 50 cycles. Scan rate: 50 mV s^{-1}. (c) CV curves of GCE, GO/GCE, Hemin/GCE, and H-ERGO/GCE in 5 mM $[Fe(CN)_6]^{3-/4-}$ containing 0.1 M KCl. Scan rate: 100 mV s^{-1}. (d) EIS spectra of GCE, GO/GCE, Hemin/GCE, and H-ERGO/GCE. Amplitude: 5 mV, frequency: 0.1 to 1 × 10^6 Hz. Right inset: enlarged high-frequency region. Upper left inset: equivalent circuit $[R_s(C_{dl}(R_{ct}Z_w))]$ fitting electrode. Rs: solution resistance, Cdl: double-layer capacitance, Rct: electron transfer resistance, Zw: diffusion resistance.

The CV curves of GCE, GO/GCE, Hemin/GCE, and H-ERGO/GCE are shown in Fig. 4(c). A pair of distinct redox peaks is observed on the GCE with a peak potential difference (ΔE_p) of 95 mV [Fig. 4(c)]. Compared with those of GCE, the CV curves of GO/GCE and Hemin/GCE display enlarged ΔE_p and reduced peak currents, indicating the impeded electron transfer between the redox probe and the electrode.[24] In contrast, the peak current of H-ERGO/GCE significantly increases with a ΔE_p of 115 mV compared with that of GCE, GO/GCE, or Hemin/GCE. The electroactive area of the electrode can be estimated using the Randles–Sevcik equation[25]

$$A = \frac{I_p}{2.69\times10^5 \times n^{3/2} \times D^{1/2} \times V^{1/2} \times C}, \tag{1}$$

where A is the electroactive surface area (cm^2), I_p is the peak current (A), $n = 1$, $D = 1.0 \times 10^{-5}$ (cm^2 s^{-1}), V is the scan rate (V s^{-1}), and C is the concentration (mol ml^{-1}) of probe molecules. The calculated electroactive surface areas are 3.28 and 5.42 mm^2 for GCE and H-ERGO/GCE, respectively. Thus, the presence of H-ERGO not only increased the electroactive area but also improved the electron transfer ability of the electrode.[26]

EIS was extensively used for studying the interfacial properties of the electrode.[27] The semicircular pattern diameter of the EIS spectrum in the high-frequency region is proportional to the electron transfer resistance (R_{et}).[28] Accordingly, the estimated R_{et} value of GCE is 45.5 Ω. The R_{et} values of Hemin/GCE (6623 Ω) and GO/GCE show significant increases, revealing that both Hemin and GO block electron transfer and reduce the electron transfer rate [Fig. 4(d)]. In contrast, the calculated R_{et} value of H-ERGO/GCE is 135.5 Ω, indicating the good electrical property of H-ERGO.

Figure 5(a) shows the CV curves of H-ERGO/GCE at different scan rates ranging from 10 to 700 mV s^{-1}. As the scan rate increases, both the anodic and cathodic currents increase [Fig. 5(b)]. Then, the redox peak current of H-ERGO/GCE increases linearly relative to the scan rate, and the electrochemical behavior of H-REGO is a surface control process.[28] In addition, the effect of pH was studied [Fig. 5(c)]. The peak potential of H-ERGO/GCE strongly depends on the pH of the electrolyte. A stable set of redox peaks can be clearly observed in the pH range from 5.5 to 8.0, but the anode and cathode peak potentials negatively shift with increasing pH. The formal potential E^{θ} of the electrode is linear with pH [Fig. 5(d)]. The slope of −55.70 mV pH^{-1} is close to the theoretical value of transferring the same number of protons and electrons in a reversible redox process (−58.60 mV pH^{-1}), indicating that this is a single-electron transfer process.[29]

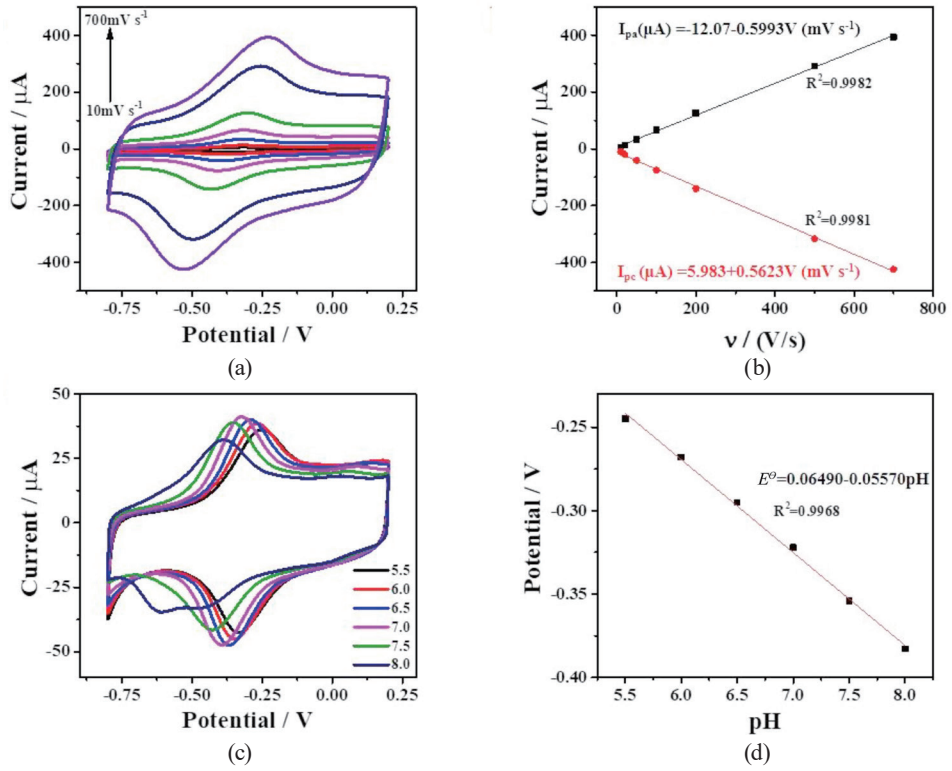

Fig. 5. (Color online) (a) CV curves of H-ERGO/GCE at different scan rates. (b) Plot of redox current of H-ERGO/GCE against scan rate. (c) CV curves of H-ERGO/GCE in 0.1 M PBS with different pHs of 5.5, 6.0, 6.5, 7.0, 7.5, and 8.0. (d) Effect of pH on the peak current.

3.4 Electrochemical performance of H-ERGO for H_2O_2 detection

Figure 6 shows the responses of GCE, ERGO/GCE, Hemin/GCE, and H-ERGO/GCE to H_2O_2. As shown in Fig. 6(a), a relatively poor electrochemical response of GCE to H_2O_2 is observed. Compared with GCE, ERGO/GCE shows an improved response with a large charging current, owing to the excellent conductivity as well as large surface area of ERGO [Fig. 6(b)]. For Hemin/GCE, the current response to H_2O_2 is significantly enhanced owing to the catalytic property of Fe^{3+} in Hemin [Fig. 6(c)]. According to previous reports, the simplified mechanism of H_2O_2 reduction by H-REGO can be expressed as the following scheme:[30]

Hemin (Fe^{3+}) + H_2O_2 → Compound I (Fe^{4+}=O) + H_2O,

Compound I (Fe^{4+} = O) + H^+ + e^- → Compound II,

Compound II + H^+ + e^- → Hemin (Fe^{3+}) + H_2O.

However, the inert surface of GCE limits the activity of the mimetic enzyme Hemin. The superior electrochemical performance of H-ERGO/GCE was demonstrated by the previous tests. Upon the addition of H_2O_2, the H-ERGO/GCE response significantly increases and it displays superior catalytic activity [Fig. 6(d)].

Figure 7 shows the electrochemical responses of GCE, ERGO/GCE, Hemin/GCE, and H-ERGO/GCE to 10 mM H_2O_2. Clearly, H-ERGO/GCE exhibits the largest response current, indicating that H-ERGO shows the highest catalytic activity for H_2O_2 reduction.

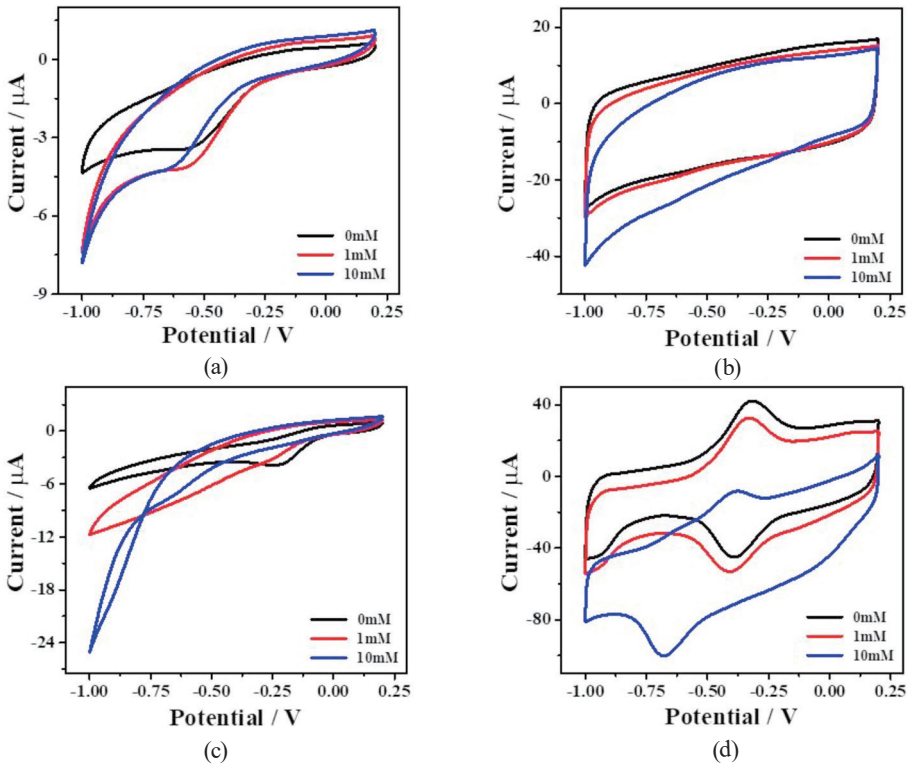

Fig. 6. (Color online) CV curves of (a) GCE, (b) ERGO/GCE, (c) Hemin/GCE, and (d) H-ERGO/GCE in 0.1 M PBS (pH 7.0) containing different H_2O_2 concentrations.

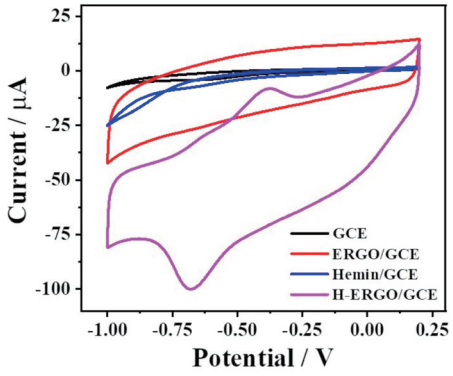

Fig. 7. (Color online) CV curves of GCE, ERGO/GCE, Hemin/GCE, and H-ERGO/GCE in 0.1 M PBS (pH 7.0) containing 10 mM H_2O_2.

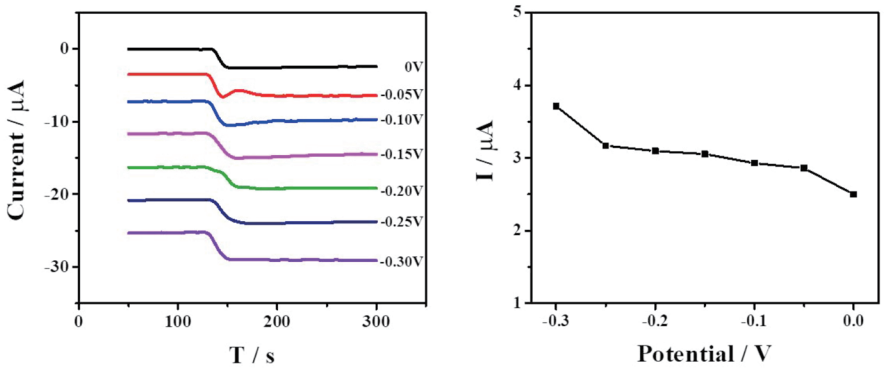

Fig. 8. (Color online) (a) Current responses of H-ERGO/GCE toward 1 mM H_2O_2 at different potentials. (b) Effect of applied potential on current.

The current responses of H-ERGO/GCE toward 1 mM H_2O_2 at different potentials were tested [Fig. 8(a)]. With the decrease in potential from 0 to −0.30 V, the current gradually increases [Fig. 8(b)]. However, at a low potential, common substances, such as urea and ascorbic acid (AA), may affect the determination of H_2O_2. Therefore, −0.15 V was selected as a suitable potential for H_2O_2 detection.

Figure 9(a) shows the response of H-ERGO/GCE to H_2O_2 in a current–time (i–t) plot at the potential of −0.15 V. Upon the addition of H_2O_2, the current increases and reaches a stable value rapidly. As shown in Fig. 9(b), the linear range for H_2O_2 detection at H-ERGO/GCE is 25 to 8850 μM, with the linear regression equation I (μA) = 0.03982 + 6.609C (mM) (R^2 = 0.9884); when the H_2O_2 concentration ranges from 8850 to 28850 μM, the linear regression equation is I (μA) = 29.59 + 2.982C (mM) (R^2 = 0.9912). When the C_{H2O2} values are below 8850 μM, H_2O_2 with relatively low concentrations can be reduced quickly at H-ERGO/GCE, producing fast response signals as shown in Fig. 9(a). Thus, a high sensitivity was obtained at H-ERGO/GCE for H_2O_2 in the range from 25 to 8850 μM. However, for C_{H2O2} ranging from 8850 to 28850 μM, a relatively low sensitivity was obtained.[31] The detection limit is 8.33 μM (S/N = 3).

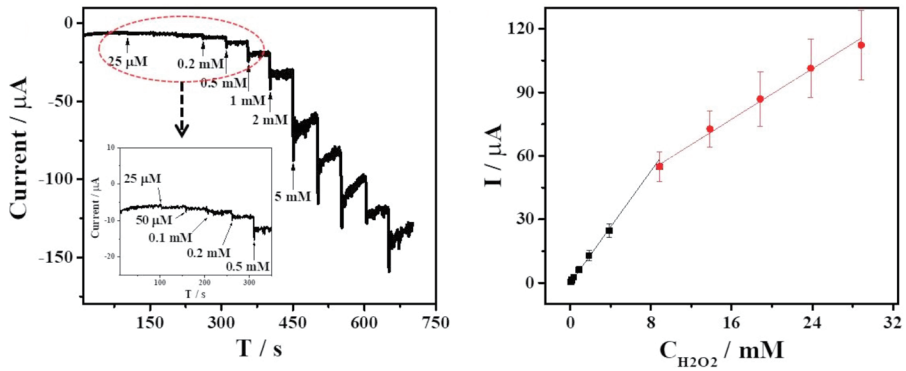

(a) (b)

Fig. 9. (Color online) (a) Amperometric response curve of H-ERGO/GCE to successive injection of H_2O_2 into 0.1 M PBS (pH 7.0). (b) Calibration curve of the reduction currents at H-ERGO/GCE against H_2O_2 concentration.

Table 1
Comparison of analytic performance of different electrochemical biosensors for H_2O_2 detection.

Electrode	Linear range (μM)	Detection limit (μM)	Reference
Au/HRP/GS/CS/GCE	5–5130	1.7	32
HRP/PTMSPA@GNRs	10–1000	0.06	33
HRP/silica matrix	20–200	3	34
Nafion/HRP/GNSs–TiO2	41–630	5.9	35
ND-NS(HRP)/ME	1000–45000	59	36
H-ERGO/GCE	25–8850; 8850–28850	8.33	This work

The fabricated H-ERGO/GCE shows a lower detection limit with a wider linear range than the previously reported H_2O_2 analytical methods (Table 1).

3.5 Selectivity, reproducibility, and stability of the H_2O_2 biosensor

To examine the applicability of the proposed biosensor in real samples, the interferences of several substances, including glucose (glu), ascorbic acid (AA), and urea, were investigated. Figure 10(a) shows the *I–t* responses upon the consecutive injection of H_2O_2 (0.2 mM), urea (1.0 mM), glu (1.0 mM), AA (1.0 mM), and H_2O_2 (0.2 mM). Clearly, these interferences show the insignificant effect of the biosensor on H_2O_2 detection, revealing the high selectivity of the proposed sensor.

Four intermittent measurements were performed to detect 0.2 mM H_2O_2, and the obtained relative standard deviation (RSD) was 2.5% [Fig. 10(b)]. The reproducibility of the biosensors was estimated by testing the response of five different electrodes towards 1 mM H_2O_2. The result indicates a satisfactory reproducibility of biosensors with an RSD of 3.7%. Moreover, the stability of the sensor was tested. The response maintained 87% of the initial value, after storage at 4 °C for one week. The good stability may result from the enzymatic mimetic properties of H-ERGO and the elimination of enzymatic denaturation problems.

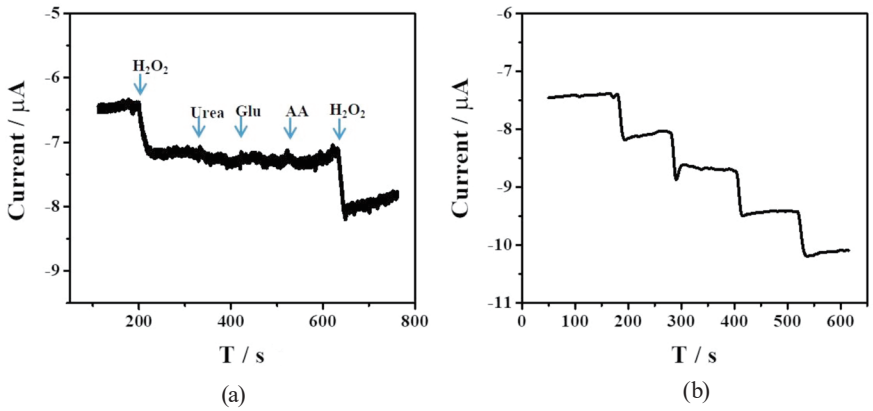

Fig. 10. (Color online) (a) *I–t* curve of H-ERGO/GCE upon successive addition of urea, glu, AA, and H_2O_2. (b) *I–t* curve of H-ERGO/GCE upon successive addition of H_2O_2.

Table 2
Recoveries of H_2O_2 in real samples (n = 3).

Samples	Added (μM)	Detected (μM)	Recovery (%)	RSD (%)
I	30	29.1	97.2	6.5
II	50	47.3	94.6	2.8
III	100	98.1	98.1	3.7

3.6 Real sample analysis

To prove its applicability, the biosensor was applied to analyze milk samples by the standard addition method.[37] The test results are summarized in Table 2. The calculated recoveries for milk samples are between 94.6 and 98.1% with RSDs below 6.5%.

4. Conclusions

We have fabricated a high-performance nonenzymatic H_2O_2 biosensor based on H-ERGO. In contrast to typical methods, the biosensor here was fabricated by the electrochemical reduction method without using a binder. A high catalytic performance toward H_2O_2 reduction was achieved by coupling Hemin with graphene. The proposed biosensor displayed good sensitivity and selectivity with high stability toward H_2O_2 detection. Furthermore, our biosensor was successfully employed to detect H_2O_2 in milk samples. The development of this type of sensor has a good prospect in the application to detection and provides a reference for more rapid detection.

Acknowledgments

We wish to thank the Natural Science Foundation of Jiangsu Province (No. BK20160490), National Natural Science Foundation of China (Nos. 21475124 and 21675065), Innovation

and Entrepreneurship Training Programs for Undergraduates (201710299095X), and Priority Academic Program Development of Jiangsu Higher Education Institutions.

References

1 M. Dynowski, G. Schaaf, D. Loque, O. Moran, and U. Luddewig: Biochem. J. **414** (2008) 53. https://doi.org/10.1042/BJ20080287
2 S. G. Rhee: Science **312** (2006) 1882. https://doi.org/10.1126/science.1130481
3 B. K. Saha, M. Y. Ali, M. Chakraborty, Z. Islam, and A. K. Hira: Pakistan J. Nutrit. **2** (2003) 36.
4 M. Valko, D. Leibfritz, J. Moncola, M. T. D. Cronin, M. Mazura, and J. Telser: Int. J. Biochem. Cell Biol. **39** (2007) 44. https://doi.org/10.1016/j.biocel.2006.07.001
5 J. Pla-Tolos, Y. Moliner-Martinez, C. Molins-Legua, and P. Campins-Falco: Sens. Actuators, B **231** (2016) 837. https://doi.org/10.1016/j.snb.2016.03.094
6 L. L. Liang, F. F. Lan, L. Li, M. Su, S. G. Ge, J. H. Yu, H. Y. Liu, and M. Yan: Biosens. Bioelectron. **82** (2016) 204. https://doi.org/10.1016/j.bios.2016.03.076
7 P. Reanpang, S. Themsirimongkon, S. Saipanya, O. Chailapakul, and J. Jakmunee: Talanta **144** (2015) 868. https://doi.org/10.1016/j.talanta.2015.07.041
8 C. Z. Wang, Y. F. E, L. Z. Fan, Z. H. Wang, H. B. Liu, Y. L. Li, S. H. Yang, and Y. L. Li: Adv. Mater. **19** (2007) 3677. https://doi.org/10.1002/adma.200701386
9 K. R. Rogers, J. Y. Becker, J. Wang, and F. Lu: Field Anal. Chem. Technol. **3** (1999) 161. https://doi.org/10.1002/(SICI)1520-6521(1999)3:3<161::AID-FACT3>3.0.CO;2-X
10 G. F. Zhang and P. K. Dasgupta: Anal. Chem. **64** (1992) 517. https://doi.org/10.1021/ac00029a013
11 C. J. Gu, F. Y. Kong, Z. D. Chen, D. H. Fan, H. L. Fang, and W. Wang: Biosens. Bioelectron. **78** (2016) 300. https://doi.org/10.1016/j.bios.2015.11.035
12 T. Lotzbeyer, W. Shuhmann, and H. L. Schmidt: J. Electroanal. Chem. **395** (1995) 341. https://doi.org/10.1016/0022-0728(95)04265-P
13 F. Valentini, L. Cristofanelli, M. Carbone, and G. Palleschi: Electrochim. Acta **63** (2012) 37. https://doi.org/10.1016/j.electacta.2011.12.027
14 S. H. Lee, D. R. Dreyer, J. H. An, A. Velamakanni, R. D. Piner, S. J. Park, Y. W. Zhu, S. O. Kim, C. W. Bielawski, and R. S. Ruoff: Macromol. Rapid Commun. **31** (2010) 281. https://doi.org/10.1002/marc.200900641
15 X. H. Zhou, L. H. Liu, X. Bai, and H. C. Shi: Sens. Actuators, B **181** (2013) 661. https://doi.org/10.1016/j.snb.2013.02.021
16 G. H. Lu, L. E Ocola, and J. H. Chen: Nanotechnology **20** (2009) 445502. https://doi.org/10.1088/0957-4484/20/44/445502
17 H. L. Guo, X. F. Wang, Q. Y. Qian, F. B. Wang, and X. H. Xia: ACS Nano **3** (2009) 2653. https://doi.org/10.1021/nn900227d
18 L. Yang, D. Liu, J. S. Huang, and T. Y. You: Sens. Actuators, B **193** (2014) 166. https://doi.org/10.1016/j.snb.2013.11.104
19 W. Lei, L. H. Wu, W. J. Huang, Q. L. Hao, Y. H. Zhang, and X. F. Xia: J. Mater. Chem. B **2** (2014) 4324. https://doi.org/10.1039/c4tb00313f
20 H. L. Zou, B. L. Li, H. Q. Luo, and N. B. Li: Sens. Actuators, B **207** (2015) 535. https://doi.org/10.1016/j.snb.2014.10.121
21 S. Stankovich, D. A. Dikin, R. D. Piner, K. A. Kohlhaas, A. Kleinhammes, Y. Y. Jia, Y. Wu, S. T. Nguyen, and R. S. Ruoff: Carbon **45** (2007) 1558. https://doi.org/10.1016/j.carbon.2007.02.034
22 F. P. Liu, J. Q. Tang, J. Xu, Y. Shu, Q. Xu, H. M. Wang, and X. Y. Hu: Biosens. Bioelectron. **86** (2016) 871. https://doi.org/10.1016/j.bios.2016.07.089
23 M. A. Raj and S. A. John: J. Phys. Chem. C **117** (2013) 4326. https://doi.org/10.1021/jp400066z
24 M. H. Zhang, R. Yuan, Y. Q. Chai, S. H. Chen, X. Zhong, H. A. Zhong, and C. Wang: RSC Adv. **2** (2012) 4639. https://doi.org/10.1039/C2RA20374J
25 M. Pacios, M. del Valle, J. Bartroli, and M. J. Esplandiu: J. Electroanal. Chem. **619** (2008) 117. https://doi.org/10.1016/j.jelechem.2008.03.019
26 W. Zhang, G. M. Xie, S. F. Li, L. S. Lu, and B. Liu: Appl. Surf. Sci. **258** (2012) 8222. https://doi.org/10.1016/j.apsusc.2012.05.025
27 X. Y. Lin, Y. N. Ni, and S. Kokot: J. Hazard. Mater. **243** (2012) 232. https://doi.org/10.1016/j.jhazmat.2012.10.026
28 H. Y. Song, Y. N. Ni, and S. Kokot: Anal. Chim. Acta **788** (2013) 24. https://doi.org/10.1016/j.aca.2013.06.016

29 A. P. Periasamy, Y. J. Chang, and S. M. Chen: Bioelectrochemistry **80** (2011) 114. https://doi.org/10.1016/j.bioelechem.2010.06.009
30 Y. Zhang, Z. Xia, H. Liu, M. J. Yang, L. L. Lin, and Q. Z. Li: Sens. Actuators, B **188** (2013) 496. https://doi.org/10.1016/j.snb.2013.07.010
31 X. X. Dong, M. Y. Li, N. N. Feng, Y. M. Sun, C. Yang, and Z. L. Xu: RSC Adv. **5** (2015) 86485. https://doi.org/10.1039/C5RA18560B
32 K. F. Zhou, Y. H. Zhu, X. L. Yang, J. Luo, C. Z. Li, and S. R. Luan: Electrochim. Acta **55** (2010) 3055. https://doi.org/10.1016/j.electacta.2010.01.035
33 S. Komathi, A. I. Gopalan, S. K. Kim, G. S. Anand, and K. P. Lee: Electrochim. Acta **92** (2013) 71. https://doi.org/10.1016/j.electacta.2013.01.032
34 S. Yang, W. Z. Jia, Q. Y. Qian, Y. G. Zhou, and X. H. Xia: Anal. Chem. **81** (2009) 3478. https://doi.org/10.1021/ac802739h
35 Y. Wang, X. L. Ma, Y. Wen, Y. Y. Xing, Z. R. Zhang, and H. F. Yang: Biosens. Bioelectron. **25** (2010) 2442. https://doi.org/10.1016/j.bios.2010.04.002
36 A. I. Gopalan, S. Komathi, G. S. Anand, and K. P. Lee: Biosens. Bioelectron. **46** (2013) 136. https://doi.org/10.1016/j.bios.2013.02.036
37 E. Akyilmaz, G. Oyman, E. Cınar, and G. Odabas: Prep. Biochem. Biotechnol. **47** (2017) 86. https://doi.org/10.1080/10826068.2016.1172235